Available online at www.sciencedirect.com

ScienceDirect

MATTER AND RADIATION AT EXTREMES

Matter and Radiation at Extremes 1 (2016) 308−315

www.journals.elsevier.com/matter-and-radiation-at-extremes

Research Article

Radiation reaction induced spiral attractors in ultra-intense colliding laser beams

Zheng Gong [a], Ronghao Hu [a], Yinren Shou [a], Bin Qiao [a], Chiaer Chen [a], Furong Xu [a], Xiantu He [a], Xueqing Yan [a,b,*]

[a] *State Key Laboratory of Nuclear Physics and Technology, and Key Laboratory of HEDP of the Ministry of Education, CAPT, Peking University, Beijing, 100871, China*

[b] *Collaborative Innovation Center of Extreme Optics, Shanxi University, Taiyuan, Shanxi, 030006, China*

Received 10 September 2016; revised 18 October 2016; accepted 27 October 2016
Available online 22 November 2016

Abstract

The radiation reaction effects on electron dynamics in counter-propagating circularly polarized laser beams are investigated through the linearization theorem and the results are in great agreement with numeric solutions. For the first time, the properties of fixed points in electron phase-space were analyzed with linear stability theory, showing that center nodes will become attractors if the classical radiation reaction is considered. Electron dynamics are significantly affected by the properties of the fixed points and the electron phase-space densities are found to be increasing exponentially near the attractors. The density growth rates are derived theoretically and further verified by particle-in-cell simulations, which can be detected in experiments to explore the effects of radiation reaction qualitatively. The attractor can also facilitate realizing a series of nanometer-scaled flying electron slices via adjusting the colliding laser frequencies.

PACS Codes: 52.38.−r; 05.45.−a; 41.85.Ct

Keywords: Radiation reaction effect; Phase space dynamics; PIC simulation

1. Introduction

The interactions of ultra-short and ultra-intense laser pulses with various plasmas can generate brilliant sources of energetic electrons, ions, X/γ-rays, and positrons with proper laser plasma parameters [1−5]. Electrons are the most fundamental particles in laser plasma interaction as electrons can be easily accelerated to relativistic velocities with laser intensities higher than 10^{18} W/cm^2 [6−8]. The electron dynamics in laser fields has been investigated thoroughly under the framework of classical electrodynamics. However, with the advent of more powerful laser facilities, laser intensities are about to achieve 10^{23} W/cm^2 [9] and electron dynamics in such intense laser fields are substantially different since here the magnitude of radiation reaction (RR) force and Lorentz force are comparable [10]. The quantum electrodynamics (QED) based numeric method [11−15] provides an explicitly self-consistent description of electron discrete emission and the corresponding radiation recoil. Semi-classical description [16,17] of radiation reaction force provides a reliable theoretical method to estimate the continuous radiation effects, avoiding the well-known self-acceleration solutions of classical models [18]. Novel phenomena beyond the framework of classical electrodynamics are predicted by the semi-classical method and

* Corresponding author. State Key Laboratory of Nuclear Physics and Technology, and Key Laboratory of HEDP of the Ministry of Education, CAPT, Peking University, Beijing, 100871, China.

E-mail address: x.yan@pku.edu.cn (X.Q. Yan).

Peer review under responsibility of Science and Technology Information Center, China Academy of Engineering Physics.

http://dx.doi.org/10.1016/j.mre.2016.10.005

QED model such as the radiation trapping [19−21], phase space contraction [22,23], QED induced stochastic effect [15,24] and e^+e^- pair production [25].

Experimental detection of radiation reaction effect could be difficult as it is almost unaccessible to measure the microscopic quantities of a single electron motion. However, with proper experimental setup, the tiny differences in electron dynamics can lead to the changes of macroscopic quantities that can be measured with available techniques [26,27]. Detecting the angular distribution changing of the electron or its emitted photon in counter-propagating laser fields provides an optimal method to qualitatively explore the signatures of radiation reaction [28,29]. Recently, γ-ray generation and pair production in counter-propagating laser fields have been investigated widely [30−32], whereas the electron spatiotemporal evolution near the attractors in intense colliding laser beams still lacks a quantitative prediction. On the other hand, for laser radiation with 1 μm wavelength, the radiation friction force changes the scenario of the electromagnetic wave interaction with matters at the intensity of $I_R \approx 10^{23}$ W/cm^2. For the laser intensity close to I_R, the electron interaction with the electromagnetic field is principally determined by a counterplay between the radiation friction and quantum effects [5,33]. When the laser intensity is higher than $I_Q = 5.75 \times 10^{23}$ (1 μm/λ) W/cm^2, the QED effects weaken the electromagnetic emission [34] and the process of photon emission becomes stochastic [11]. Provided that the QED induced radiation is weakened and the stochastic effect is indifferent under the laser intensity lower than I_Q, the classical radiation reaction approach still gives us valid results. In this paper, we utilized the classical radiation reaction model to investigate the electron dynamics in counter-propagating laser fields. The presented electron spatiotemporal evolution was dominantly affected by the fixed points in electron phase-space and the analytical solutions of electron dynamics were obtained with linear stability theory [35]. It is found that the spiral attractors induced by radiation reaction can lead to exponential growth of in situ density and the analytic growth rates were given and compared with numeric solutions.

2. Theoretical analysis

For simplicity and generality, the counter propagating laser pulses are described by infinite plane wave vector potential, $\boldsymbol{A}_1 = a_0[\sin(t-x)\widehat{\boldsymbol{y}} + \cos(t-x)\widehat{\boldsymbol{z}}]$ and $\boldsymbol{A}_2 = a_0[\sin(t+x)\widehat{\boldsymbol{y}} + \cos(t+x)\widehat{\boldsymbol{z}}]$; $\widehat{\boldsymbol{y}}$(or $\widehat{\boldsymbol{z}}$) is the unit vector in y (or z) direction; a_0 is the normalized laser amplitude ($a_0 = eE_0/m_e c w_0$), where e and m_e are the electron charge and mass, E_0 and w_0 are the electric amplitude and frequency, c is the speed of light, respectively; x and t are normalized to c/w_0 and w_0, respectively. The electromagnetic standing wave (SW) field can be deduced as $\boldsymbol{E} = -\partial\boldsymbol{A}/\partial t = -2a_0\cos(x)\cos(t)\widehat{\boldsymbol{y}} + 2a_0\cos(x)\sin(t)\widehat{\boldsymbol{z}}$ and $\boldsymbol{B} = \nabla\times\boldsymbol{A} = 2a_0\sin(x)\cos(t)\widehat{\boldsymbol{y}} - 2a_0\sin(x)\sin(t)\widehat{\boldsymbol{z}}$ from the whole region vector potential $\boldsymbol{A} = \boldsymbol{A}_1 + \boldsymbol{A}_2$.

First of all, considering the condition without RR recoil, electron dynamics in phase-space x-p_x is determined by relativistic Lorentz force $\mathrm{d}\boldsymbol{p}/\mathrm{d}t = \partial\boldsymbol{A}/\partial t - \boldsymbol{v}\times(\nabla\times\boldsymbol{A})$. As SW field is independent of y and z, there are two invariant equations:

$$\frac{\mathrm{d}p_y}{\mathrm{d}t} = \frac{\partial A_y}{\partial t} + v_x\frac{\partial A_y}{\partial x} = \frac{\mathrm{d}A_y}{\mathrm{d}t}, \tag{1}$$

$$\frac{\mathrm{d}p_z}{\mathrm{d}t} = \frac{\partial A_z}{\partial t} + v_x\frac{\partial A_z}{\partial x} = \frac{\mathrm{d}A_z}{\mathrm{d}t}. \tag{2}$$

Assuming at initial time $p_y\big|_{t=0} = A_y\big|_{t=0}$ ($p_z\big|_{t=0} = A_z\big|_{t=0}$), the above conservative relations tell us that $p_z \equiv A_z = 2a_0\cos(x)\cos(t)$ ($p_y \equiv A_y = 2a_0\cos(x)\sin(t)$). For the relativistic factor $\gamma = \sqrt{1+p_x^2+4a_0^2\cos^2(x)}$, the nonlinear differential equation in x-p_x space is derived as:

$$\frac{\mathrm{d}x}{\mathrm{d}t} = \frac{p_x}{\gamma} = \frac{p_x}{\sqrt{1+p_x^2+4a_0^2\cos^2(x)}}, \tag{3}$$

$$\frac{\mathrm{d}p_x}{\mathrm{d}t} = -v_yB_z + v_zB_y = \frac{4a_0^2\cos(x)\sin(x)}{\sqrt{1+p_x^2+4a_0^2\cos^2(x)}}. \tag{4}$$

From the time-independent nonlinear relationship Eqs. (3) and (4) (i.e., autonomous nonlinear system in mathematics), we can exactly find that the relativistic factor is a conservative Hamiltonian:

$$H = \gamma = \sqrt{1+p_x^2+4a_0^2\cos^2(x)}, \tag{5}$$

since $\mathrm{d}H/\mathrm{d}t = \partial H/\partial t \equiv 0$ is validated from the corresponding canonical equation $\mathrm{d}x/\mathrm{d}t = \partial\gamma/\partial p_x = f(x, p_x)$ and $\mathrm{d}p_x/\mathrm{d}t = -\partial\gamma/\partial x = g(x, p_x)$, which are completely equivalent with Eqs. (3) and (4). The Hamiltonian H is symmetrical and periodic, and note that there are some special solutions of these differential equations when the initial value (x^*, p_x^*) satisfies $f(x^*, p_x^*) = 0$ and $g(x^*, p_x^*) = 0$. This is the constant solution $(x, p_x) \equiv (x^*, p_x^*)$. A constant solution such as this is called an equilibrium solution or equilibrium point for the equation [35]. Subsequently there are four equilibrium points (x^*, p_x^*) at electric nodes (π/2, 0), (3π/2, 0) and antinodes (0, 0), (π, 0) in a SW period, as shown in Fig. 1(a). The property of an equilibrium point in the nonlinear system can be classified via its linear approximation near the equilibrium point. The Jacobian matrix is a linearization method via calculating the first partial derivatives, which facilitates us to investigate the property of the equilibrium point [35,36]. To determine whether the equilibrium point is stable or not, by making the disturbance expansion near $(x-x^*, p_x-p_x^*)$ and dropping quadratic terms to linearize Eqs. (3) and (4), the characteristic Jacobian matrix **Ja** at the equilibrium point (x^*, p_x^*) is obtained:

$$\mathbf{Ja} = \begin{pmatrix} \dfrac{\partial f(x,p_x)}{\partial x} & \dfrac{\partial f(x,p_x)}{\partial p_x} \\ \dfrac{\partial g(x,p_x)}{\partial x} & \dfrac{\partial g(x,p_x)}{\partial p_x} \end{pmatrix}_{x^*,p_x^*} = \begin{pmatrix} 0 & \dfrac{1}{\gamma} \\ \dfrac{4a_0^2\cos(2x)}{\gamma} & 0 \end{pmatrix}_{x^*,p_x^*}. \tag{6}$$

For the electric node $x^* = \pi/2$ or $3\pi/2$, the trace and determinant of Jacobian matrix are $\mathrm{tr}(\mathbf{Ja}) = 0$ and

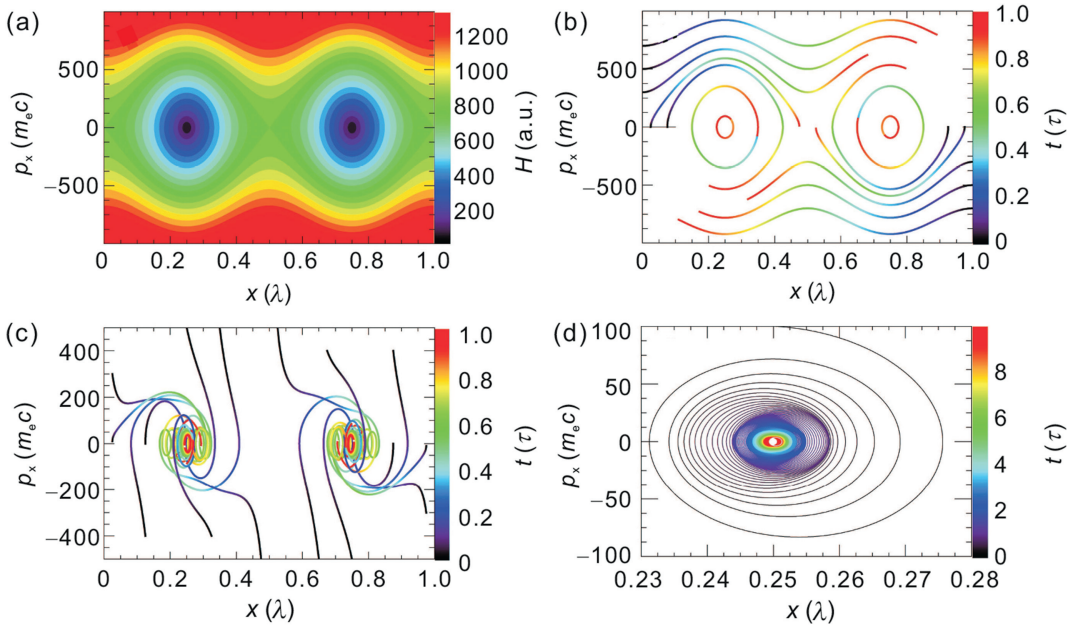

Fig. 1. Equation integration result at the laser field amplitude $a_0 = 300$. (a) The conservative Hamiltonian (H) for electrons satisfying initial condition $p_y|_{t=0} = A_y|_{t=0}$ ($p_z|_{t=0} = A_z|_{t=0}$), with RR effect ignored. For denotation simplicity, the unit in x-direction is laser wavelength λ rather than inverse of wave number $\lambda/2\pi$. (b) Trajectories of electron in phase-space (x, p_x) without RR, which illustrates the node ($x = 0.25\lambda$ or 0.75λ) acts as a center. Color denotes the temporal variation in laser period τ. (c) Same as (b), but RR effect included, where the node behaves like a attractor but the spiral phenomenon doesn't exhibit. (d) The electron approaches to one node spirally when it is close to the node.

$\det(\mathbf{Ja}) = 4a_0^2 > 0$, which manifest that ($\pi$/2, 0), (3$\pi$/2, 0) are centers without any source or sink effect when excluding RR [35]. The counterparts at $x^* = 0$ or π, $\mathrm{tr}(\mathbf{Ja}) = 0$ and $\det(\mathbf{Ja}) = -\frac{4a_0^2}{1+4a_0^2} < 0$, indicate that the antinodes (0, 0), (π, 0) are unstable saddle points where a tiny disturbance can trigger drastic turbulence growth. In Fig. 1(b), the orbits of electrons without RR, initially satisfying the condition $p_\perp|_{t=0} = A_\perp|_{t=0}$, are attained by integrating Eqs. (3) and (4). This analysis method with respect to the property of the equilibrium point can be carried forward to RR circumstance directly.

Considering the reasonability and causality of the RR effect, in the paper we use the Landau Lifshitz (LL) force [37] for RR form to explore its influence on the equilibrium point. The spatial components of LL force are:

$$\begin{aligned}\boldsymbol{F}_{\mathrm{LL}} = &-\frac{4\pi r_e}{3\lambda}\left\{\gamma\left[\left(\frac{\partial}{\partial t}+\boldsymbol{v}\cdot\nabla\right)\boldsymbol{E}+\boldsymbol{v}\times\left(\frac{\partial}{\partial t}+\boldsymbol{v}\cdot\nabla\right)\boldsymbol{B}\right]\right\}\\ &+\frac{4\pi r_e}{3\lambda}\left\{\left[(\boldsymbol{E}+\boldsymbol{v}\times\boldsymbol{B})\times\boldsymbol{B}+(\boldsymbol{v}\cdot\boldsymbol{E})\boldsymbol{E}\right]\right.\\ &\left.-\gamma^2\left[(\boldsymbol{E}+\boldsymbol{v}\times\boldsymbol{B})^2-(\boldsymbol{v}\cdot\boldsymbol{E})^2\right]\boldsymbol{v}\right\},\end{aligned} \tag{7}$$

where $\boldsymbol{p}$ is the electron momentum, $r_e \equiv e^2/mc^2 \approx 2.8\times10^{-15}$ m is the classical electron radius, $\lambda = 2\pi c/w_0$ is the pulse wavelength, and dimensionless quantities are used for convenience. Here the momentum is in the unit of mc, the electric and magnetic fields are in units of mw_0c/e and mw_0c^2/e respectively. The first term of Eq. (7), the one containing the "total" time derivative of the electromagnetic field is neglected in calculation. Since RR is usually considered in ultra-relativistic condition $\gamma \gg 1$, the last term (proportional to γ^2) dominates over the whole LL force. Analogous to the case without RR, the corresponding Jacobian matrix with $\boldsymbol{F}_{\mathrm{LL}}$ is estimated as:

$$\mathbf{Ja} \approx \begin{pmatrix} 0 & \frac{1}{\gamma} \\ \frac{4a_0^2\cos(2x)}{\gamma} & -\frac{4\pi r_e}{3\lambda}2a_0^2\gamma \end{pmatrix}_{x^*,p_x^*}. \tag{8}$$

Using the classification principle in the trace-determinant plane, antinode (0, 0) or (π, 0) still behaves the same as the unstable saddle point with no RR case. However, at node (π/2, 0) or (3π/2, 0), where $\mathrm{tr}(\mathbf{Ja}) = -\frac{4\pi r_e}{3\lambda}2a_0^2\sqrt{1+4a_0^2} < 0$ and $\det(\mathbf{Ja}) = 4a_0^2 > 0$, the node's behavior converts from the center to the spiral sink when RR force is taken into account. As shown in Fig. 1(c), the electrons initially far from the node are attracted by it violently while they are experiencing swift movement in phase-space. This can be seen as electrons can no longer stay in the original height when friction (RR) exerts on them to dissipate their energy and eventually they fall to the valley bottom (spiral sink node). Since the RR force in the above model where electrons initially far from the equilibrium node is comparable with the Lorentz force at $a_0 = 300$ and $\gamma \approx 500$ considering estimation $\boldsymbol{F}_{\mathrm{LL}} \sim -\frac{4\pi r_e}{3\lambda}\gamma^2 a_0^2$, electrons move to the sink node swiftly rather than approach to the sink node spirally. The electron initially close to the node behaves as spiral sink characteristic regularly in Fig. 1(d), which agrees well with the analysis of Eq. (8). Under one-order perturbation approximation, the

dynamical differential equation at $(\tilde{x},\tilde{p_x}) = (x - x^*, p_x - p_x^*)$ is expressed by linear algebra equation $\lambda \boldsymbol{X} = \boldsymbol{A}\boldsymbol{X}$, here $\boldsymbol{X} = (\tilde{x},\tilde{p_x})^{\mathrm{T}}$ and $\boldsymbol{A} = \mathbf{Ja}$. The general solution $\boldsymbol{X} = \alpha \bullet \exp(\lambda_+ t)\boldsymbol{X}_1 + \beta \bullet \exp(\lambda_- t)\boldsymbol{X}_2$ illustrates the electron trajectories in x-p_x phase space, where $\lambda_{+(-)}$ is the eigenvalue of matrix $\boldsymbol{A}$, $\alpha\,(\beta)$ is the undefined constant and $\boldsymbol{X}_1\,(\boldsymbol{X}_2)$ is the eigenvector. After some miscellaneous calculations, eigenvalues $\lambda_\pm = -2\frac{4\pi r_e}{3\lambda}\gamma a_0^2 \pm 2a_0 i$ denotes the eigenvectors' amplitudes, and the decreasing rate $\Re(\lambda_\pm) = -2\frac{4\pi r_e}{3\lambda}\gamma a_0^2$. In the above series of derivation, we concentrate on the integral variation presuming the system is autonomous and in consequence instantaneous variation of SW field $\sin^2(t)$ and $\cos^2(t)$ are replaced by 0.5 for period average effect. Previously Tambrini et al. [23] and Lehnman et al. [22] qualitatively summarized the entropy differential $\mathrm{d}S/\mathrm{d}t = \int \mathrm{d}^3x\mathrm{d}^3pf\nabla_p \bullet \boldsymbol{F}_{\mathrm{LL}} \leqslant 0$, and the estimated characteristic attraction time $\sim \left[\frac{4\pi r_e}{3\lambda}\gamma a_0^2\right]^{-1}$ [22] are in good agreement with our linearized derivation. Therefore considering the conservation of quantity and amplitude decay, the 2D phase volume contraction ratio is estimated as $\exp(-2|\lambda_\pm|t)$.

3. Simulation results

To testify the numerical decay ratio, we took the advantage of one-dimension Particle in Cell (PIC) program EPOCH [38,39] to simulate the electron motion. The Lorentz force combined with LL force was realized in particle pusher model of EPOCH source code utilizing the method in Ref. [40]. The SW fields $\boldsymbol{E} = -2a_0\cos\left(\frac{2\pi}{\lambda}x\right)\cos(\omega t)\widehat{\boldsymbol{y}} + 2a_0\cos\left(\frac{2\pi}{\lambda}x\right)\sin(\omega t)\widehat{\boldsymbol{z}}$ and $\boldsymbol{B} = 2a_0\sin\left(\frac{2\pi}{\lambda}x\right)\cos(\omega t)\widehat{\boldsymbol{y}} - 2a_0\sin\left(\frac{2\pi}{\lambda}x\right)\sin(\omega t)\widehat{\boldsymbol{z}}$ were established by counter-propagation circularly polarized (CP) infinite plane wave. Meanwhile, simulation region $x \in [0,\ \lambda]$ was divided into 10^5 cells. As the perturbation approximation method is valid near the node, we initialized 10^7 electrons uniformly distributed in $\left(\frac{p_x}{a_0 m_e c}\right)^2 + \left[\frac{4\pi(x-0.75\lambda)}{\lambda}^2\right] \leqslant (0.02\pi)^2$ to explore the phase volume contraction ratio. Supposing the electron bunch was so rare that the space charge interaction was incomparable with SW field, the collective force was neglected in our PIC simulation by setting the electron as the tracer particle. As shown in Fig. 2, RR induced phase space evolution during $0 < t < 4\tau$ is exhibited for different SW amplitude $a_0 = 100$, 300, 500, where $\tau = 2\pi/\omega$ is the laser period. The derived ratio $\exp(-2|\lambda_\pm|t) = \exp\left(-\frac{16\pi r_e}{3\lambda}\gamma a_0^2 t\right)$ implies that the contraction is sensitive with amplitude a_0. The $a_0 = 500$ case illustrates that electrons are immediately trapped to the attractor (spiral node $(0,\ 0.75\lambda)$) and they are accumulated to extreme dense state after several laser periods. However, under $a_0 = 100$ circumstance, the contraction phenomenon is negligible and this bunch still distributes in a relatively large elliptical region at $t = 4\tau$. In-between the phase-space variation is observable but not so drastic for $a_0 = 300$, which is in accordance with precedent predicted threshold of radiation reaction dominant regime in Refs. [5,33].

In addition, we recorded the spiral node density evolution for different amplitude a_0 during $0 < t < 9\tau$, as shown in Fig. 3(a). The theoretical line $n_t = n_0\exp\left(\frac{16\pi r_e}{3\lambda}\gamma a_0^2 t\right)$ is deduced utilizing the inverse of contraction ratio $\exp(-2|\lambda_\pm|t)$, where γ is estimated by electron initial Hamiltonian $\gamma \sim \sqrt{1 + 2a_0\frac{2\pi}{\lambda}0.005\lambda}$. When the amplitude of SW field is

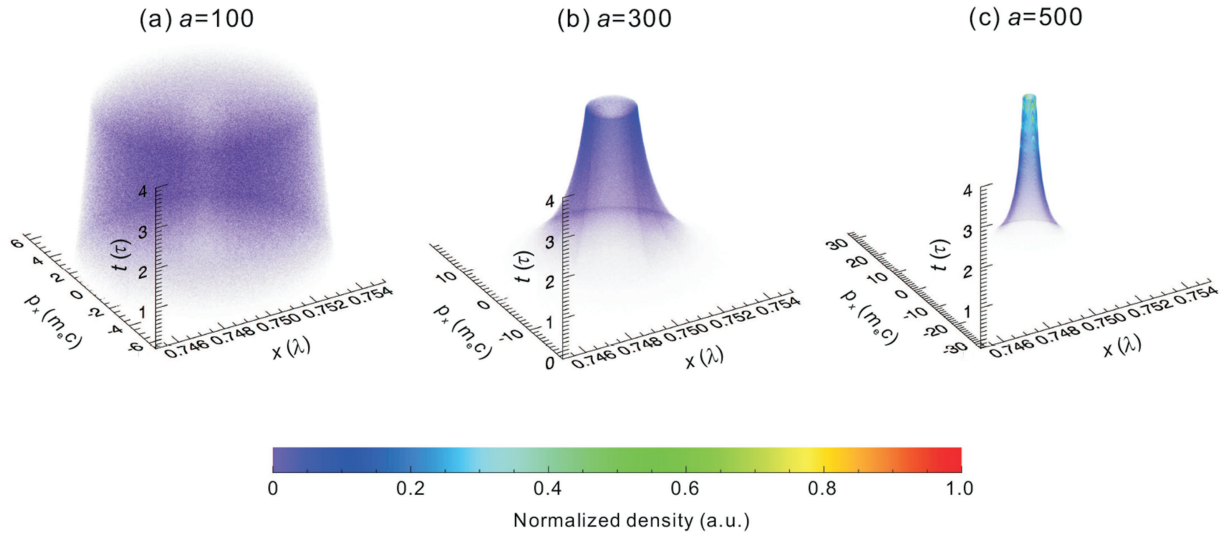

Fig. 2. (a) The electrons phase-space (x, p_x) temporal evolution at normalized laser intensity $a_0 = 100$ during $0 < t < 4\tau$. (b, c) The same as (a) with $a_0 = 300$ and $a_0 = 500$, respectively.

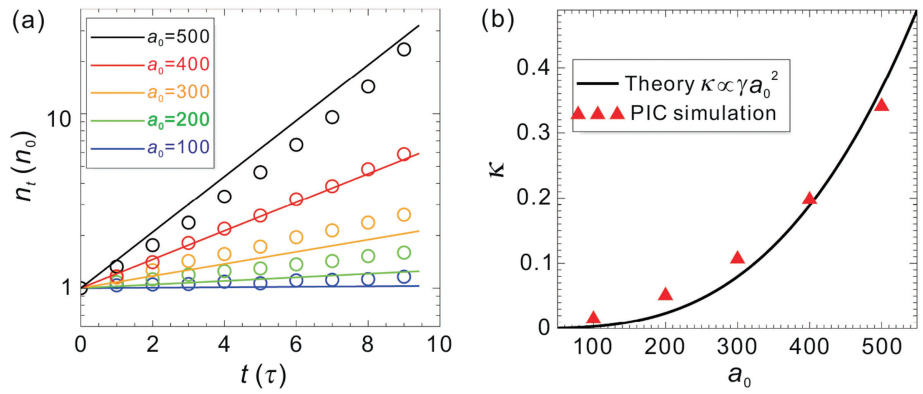

Fig. 3. (a) The normalized density variation with time at the spiral node. Solid lines present the theoretical prediction $n_t = n_0 \exp\left(\frac{16\pi r_e}{3\lambda}\gamma a_0^2 t\right)$, circles indicate results from PIC with classic LL reaction force. Different colors correspond to different pulse amplitudes a_0. (b) Solid black line shows the density growth ratio in theoretical form $\kappa = \frac{\mathrm{d}(\ln n_t)}{\mathrm{d}t} = \frac{16\pi r_e}{3\lambda}\gamma a_0^2$ while the red triangles denote the counterpart of PIC simulation results.

small enough for $a_0 = 100$ and 200, Taylor expansion of exponential growth ratio $\exp\left(\frac{16\pi r_e}{3\lambda}\gamma a_0^2 t\right) \approx 1 + \frac{16\pi r_e}{3\lambda}\gamma a_0^2 t$ indicates that the density of attractor point n_t is proportional to time t. The density growth rate can be defined as:

$$\kappa = \frac{\mathrm{d}(\ln n_t)}{\mathrm{d}t} = \frac{16\pi r_e}{3\lambda}\gamma a_0^2, \tag{9}$$

which is illustrated in Fig. 3(b) and the simulation results are in good agreement with Eq. (9). The evolution prediction exhibits its exponential growth property where a little increment of a_0 leads to substantial density accumulation in the attractor. The PIC simulation results demonstrate that the attractor density evolution is exactly determined by the RR force format and this may provide us a potential method to detect the LL force format experimentally.

Above discussion is mainly dedicated to the electron's property in vicinity of the attractor. Without loss of generality, it is essential to think over the initial condition $p_\perp\big|_{t=0} \neq A_\perp\big|_{t=0}$ where the electron relativistic factor γ is no longer conserved. Considering the realistic interaction between plasma and colliding laser pulse, we place 100000 electrons whose spatial distribution is random in x-direction and temperature is 50 MeV to simulate their behavior under periodic SW field. There both linearly polarized (LP) ($a_0 = 300\sqrt{2}$) and CP ($a_0 = 300$) are included. The Poincaré plots for different polarizations and with or without RR are shown in Fig. 4. Without RR recoil in Fig. 4(a)

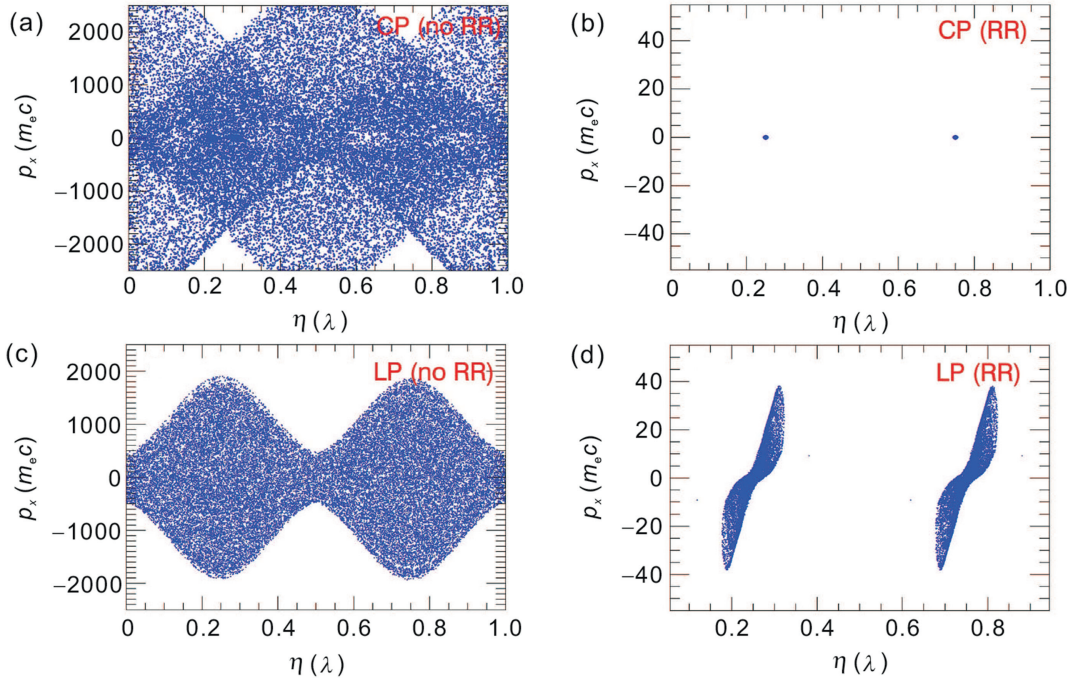

Fig. 4. Poincaré plots p_x vs η for (a) CP without RR, (b) CP with RR, and (c) LP without RR (d) LP with RR. Defining $\eta = x \bmod \lambda$, at times $t = n\tau$, $n = 0, 1 \ldots$. The plots show 100 trajectories for t from 500τ to 1000τ.

and (c), both CP and LP demonstrate the Hamiltonian chaos and the global stochastic behavior are observed. While taking account of radiation damping, both systems of CP and LP become dissipative and they switch from Hamiltonian chaos [41] to attractor behavior. The comprehensive explanation about LP condition was proposed by Lehmann in Ref. [22]. It illustrates that phase space stochastic heating turning into stranger attractor due to RR force in SW field. In RR damping circumstance shown in Fig. 4(b) and (d), the phase space contraction phenomenon for CP is much more significant than that for LP and most of the section points locate in the spiral sink node in Fig. 4(b), which indicates the regular stable attractor emerges in x-p_x phase space. Consequently, the electrons in linearly polarized SW field can be dispersed away from the electric node while the regular attractor in CP case induced cooling effect is prone to constrain electrons more tightly, where the spiral sink effect plays an important role. Meanwhile, the e^-e^+ pair plasma generation from CP is less efficient than LP due to the dispersed electrons with higher energy and emission probability [32].

4. Potential application

In addition, we outline some potential applications of spiral attractor caused by RR effect. Suppose that there is a bunch of static electrons irradiated by CP pulses from both sides in the inertial frame S', as shown in Fig. 5(a). The frame S' is moving with velocity u in the $+x$ direction with respect to the laboratory frame S. In 2D PIC simulation, a bunch of electrons are initialized with normalized energy $\gamma = 100$ moving along the x-direction with velocity $u = 1 - 1/\gamma^2$ and the CP laser pulses with amplitude $a_0 = 300$ from left and right boundaries are set as infinite plane wave whose circular frequencies are $\omega_1 = 2\gamma\omega_0$ and $\omega_2 = \omega_0/(2\gamma)$ respectively (ω_0 is the frequency corresponding to 1 μm wavelength). The simulation territory is a 20 μm × 2 μm rectangle divided by 200000 × 200 cells. Utilizing Doppler shift formulas, in S' frame laser frequencies are $\omega_1' = \omega_0$ and $\omega_2' = \omega_0$ as shown in Fig. 5(a). A similar simulation as above have been done in frame S' to accomplish periodic electron slices with length $\delta l < 1$ μm due to the spiral sink node attractive effect. In the laboratory frame, the length

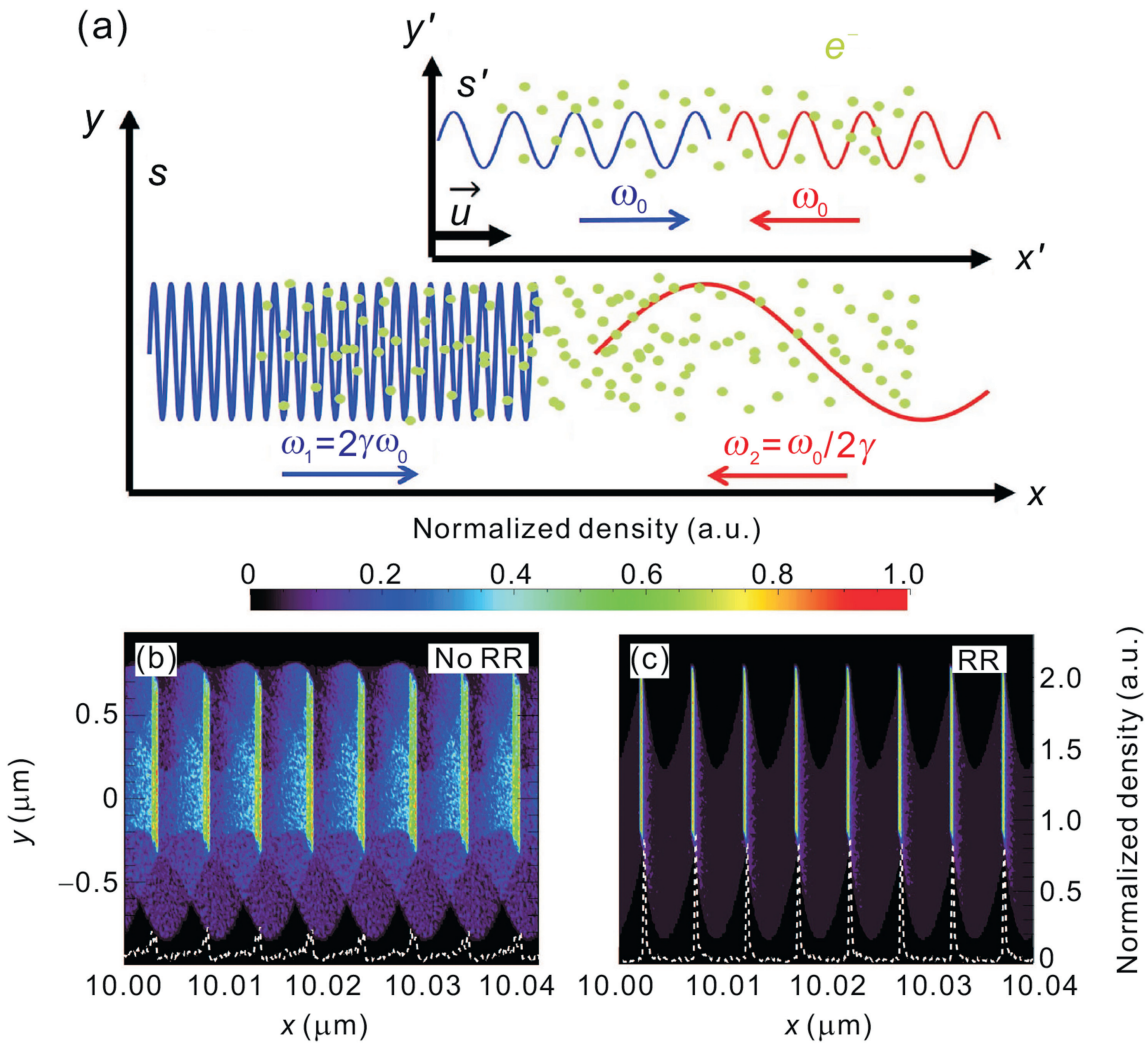

Fig. 5. (a) Schematic of the Doppler shift of colliding electromagnetic wave from inertial frame to laboratory frame. (b, c) The snapshots of electron density distributions with or without RR effect respectively. The white dashed lines denote values obtained in the section of $y = 0$.

of these slices can be calculated as $\delta l/\gamma < 10$ nm through Lorentz transformation, which is in perfect agreement with the result in Fig. 5(c) ($\delta l \approx 1$ nm). When ignoring RR effect, the SW nodes without attractive behavior cannot confine electrons in small areas so that the nanometer-scale electron slice is difficult to realize in Fig. 5(b). The parameters of the slices in Fig. 5(c) can be determined through adjusting the frequencies ω_1 and ω_2. Supposing $\omega_1 > \omega_2$ and $\varepsilon \gg 1$, the electron slice normalized directional energy $\varepsilon = \sqrt{\omega_1/(4\omega_2)}$ and its length $\delta \ll 2\pi c/(\varepsilon\sqrt{\omega_1\omega_2})$. Such a series of ultrashort and nano-bunched electron slices can be used to generate coherent transition radiation [42] and a train of attosecond X-ray pulses through coherent Thomson backscattering [43].

5. Conclusions and outlook

We proposed a novel analytic method to investigate electron dynamics in ultra-intense counter-propagating laser fields. Utilizing the linear stability theory, we found that spiral attractors emerge in electron phase-space when the classical radiation reaction is taken into account. The electrons are spirally approaching the attractors and the electron densities nearby grow exponentially. The growth rates were given theoretically, which are proportional to the laser intensities. Experimentally measuring these growth rates can provide a quantitative way to diagnose the formula of radiation reaction force.

Acknowledgements

The work has been supported by the National Basic Research Program of China (Grant No. 2013CBA01502), NSFC (Grant No. 11535001) and National Grand Instrument Project (2012YQ030142). The PIC code Epoch was in part funded by the UK EPSRC grants EP/G054950/1, EP/G056803/1, EP/G055165/1 and EP/M022463/1. Our simulations were carried out in Max Planck Computing and Data Facility and Shanghai Super Computation Center. The author Z. Gong acknowledges useful discussion with S.V. Bulanov and H.X. Chang. Z. Gong and R.H. Hu contributed equally to this work.

References

[1] G.A. Mourou, T. Tajima, S.V. Bulanov, Optics in the relativistic regime, Rev. Mod. Phys. 78 (2006) 309–371.
[2] E. Esarey, C.B. Schroeder, W.P. Leemans, Physics of laser-driven plasma-based electron accelerators, Rev. Mod. Phys. 81 (2009) 1229–1285.
[3] A. Macchi, M. Borghesi, M. Passoni, Ion acceleration by superintense laser-plasma interaction, Rev. Mod. Phys. 85 (2013) 751–793.
[4] S. Corde, K. Ta Phuoc, G. Lambert, R. Fitour, V. Malka, et al., Femtosecond X-rays from laser-plasma accelerators, Rev. Mod. Phys. 85 (2013) 1–48.
[5] A. Di Piazza, C. Müller, K. Hatsagortsyan, C. Keitel, Extremely high-intensity laser interactions with fundamental quantum systems, Rev. Mod. Phys. 84 (2012) 1177.
[6] P. Gibbon, Short Pulse Laser Interactions with Matter, World Scientific Publishing Company, 2004.
[7] J. Meyer-ter Vehn, A. Pukhov, Z.-M. Sheng, Relativistic laser plasma interaction, in: Atoms, Solids, and Plasmas in Super-intense Laser Fields, Springer, 2001, pp. 167–192.
[8] T. Toncian, C. Wang, E. McCary, A. Meadows, A. Arefiev, et al., Non-maxwellian electron distributions resulting from direct laser acceleration in near-critical plasmas, Matter Radiat. Extrem. 1 (2016) 82–87.
[9] G. Mourou, T. Tajima, More intense, shorter pulses, Science 331 (2011) 41–42.
[10] S. Bulanov, T.Z. Esirkepov, M. Kando, H. Kiriyama, K. Kondo, Relativistically strong electromagnetic radiation in a plasma, J. Exp. Theor. Phys. 122 (2016) 426–433.
[11] R. Duclous, J.G. Kirk, A. Bell, Monte Carlo calculations of pair production in high-intensity laser-plasma interactions, Plasma Phys. Control. Fusion 53 (2011) 015009.
[12] C. Ridgers, J. Kirk, R. Duclous, T. Blackburn, C. Brady, et al., Modelling gamma-ray photon emission and pair production in high-intensity laser-matter interactions, J. Comput. Phys. 260 (2014) 273–285.
[13] A. Bell, J.G. Kirk, Possibility of prolific pair production with high-power lasers, Phys. Rev. Lett. 101 (2008) 200403.
[14] A. Di Piazza, K.Z. Hatsagortsyan, C.H. Keitel, Quantum radiation reaction effects in multiphoton compton scattering, Phys. Rev. Lett. 105 (2010) 220403.
[15] N. Neitz, A. Di Piazza, Stochasticity effects in quantum radiation reaction, Phys. Rev. Lett. 111 (2013) 054802.
[16] I.V. Sokolov, N.M. Naumova, J.A. Nees, G.A. Mourou, V.P. Yanovsky, Dynamics of emitting electrons in strong laser fields, Phys. Plasmas 16 (2009) 093115.
[17] T. Nakamura, J.K. Koga, T.Z. Esirkepov, M. Kando, G. Korn, et al., High-power γ-ray flash generation in ultraintense laser-plasma interactions, Phys. Rev. Lett. 108 (2012) 195001.
[18] J.D. Jackson, Classical Electrodynamics, Wiley, 1999.
[19] L.L. Ji, A. Pukhov, I.Y. Kostyukov, B.F. Shen, K. Akli, Radiation-reaction trapping of electrons in extreme laser fields, Phys. Rev. Lett. 112 (2014) 145003.
[20] A. Gonoskov, A. Bashinov, I. Gonoskov, C. Harvey, A. Ilderton, et al., Anomalous radiative trapping in laser fields of extreme intensity, Phys. Rev. Lett. 113 (2014) 014801.
[21] T.Z. Esirkepov, S.S. Bulanov, J.K. Koga, M. Kando, K. Kondo, et al., Attractors and chaos of electron dynamics in electromagnetic standing waves, Phys. Lett. A 379 (2015) 2044–2054.
[22] G. Lehmann, K. Spatschek, Phase-space contraction and attractors for ultrarelativistic electrons, Phys. Rev. E 85 (2012) 056412.
[23] M. Tamburini, F. Pegoraro, A. Di Piazza, C.H. Keitel, T.V. Liseykina, et al., Radiation reaction effects on electron nonlinear dynamics and ion acceleration in laser-solid interaction, Nucl. Instrum. Methods Phys. Res. Sect. A 653 (2011) 181–185.
[24] M. Vranic, T. Grismayer, R.A. Fonseca, L.O. Silva, Quantum radiation reaction in head-on laser-electron beam interaction, New J. Phys. 18 (2016) 073035.
[25] S. Bulanov, V. Mur, N. Narozhny, J. Nees, V. Popov, Multiple colliding electromagnetic pulses: A way to lower the threshold of e^+e^- pair production from vacuum, Phys. Rev. Lett. 104 (2010) 220404.
[26] T.G. Blackburn, C.P. Ridgers, J.G. Kirk, A.R. Bell, Quantum radiation reaction in laser electron-beam collisions, Phys. Rev. Lett. 112 (2014) 015001.
[27] T. Heinzl, C. Harvey, A. Ilderton, M. Marklund, S.S. Bulanov, et al., Detecting radiation reaction at moderate laser intensities, Phys. Rev. E 91 (2015) 023207.
[28] A.G.R. Thomas, C.P. Ridgers, S.S. Bulanov, B.J. Griffin, S.P.D. Mangles, Strong radiation-damping effects in a gamma-ray source generated by the interaction of a high-intensity laser with a wakefield-accelerated electron beam, Phys. Rev. X 2 (2012) 041004.
[29] H. Wang, X. Yan, M. Zepf, Signatures of quantum radiation reaction in laser-electron-beam collisions, Phys. Plasmas 22 (2015) 093103.
[30] E. Nerush, I.Y. Kostyukov, A. Fedotov, N. Narozhny, N. Elkina, et al., Laser field absorption in self-generated electron-positron pair plasma, Phys. Rev. Lett. 106 (2011) 035001.

[31] H.X. Chang, B. Qiao, Z. Xu, X.R. Xu, C.T. Zhou, et al., Generation of overdense and high-energy electron-positron-pair plasmas by irradiation of a thin foil with two ultraintense lasers, Phys. Rev. E 92 (2015).

[32] M. Jirka, O. Klimo, S.V. Bulanov, Z.T. Esirkepov, E. Gelfer, et al., Electron dynamics and $e^{-}e^{+}$ production by colliding laser pulses, Phys. Rev. E 93 (2016).

[33] S.V. Bulanov, T.Z. Esirkepov, M. Kando, J. Koga, K. Kondo, et al., On the problems of relativistic laboratory astrophysics and fundamental physics with super powerful lasers, Plasma Phys. Rep. 41 (2015) 1−51.

[34] J.G. Kirk, A. Bell, I. Arka, Pair production in counter-propagating laser beams, Plasma Phys. Control. Fusion 51 (2009) 085008.

[35] M.W. Hirsch, S. Smale, R.L. Devaney, Differential Equations, Dynamical Systems, and an Introduction to Chaos, Academic Press, 2012.

[36] D. Jordan, P. Smith, Nonlinear Ordinary Differential Equations: An Introduction for Scientists and Engineers, Oxford University Press on Demand, 2007.

[37] L. Landau, Em lifshitz the classical theory of fields, Course Theor. Phys. 2 (1975).

[38] T. Arber, K. Bennett, C. Brady, A. Lawrence-Douglas, M. Ramsay, et al., Contemporary particle-in-cell approach to laser-plasma modelling, Plasma Phys. Control. Fusion 57 (2015) 113001.

[39] C. Ridgers, C.S. Brady, R. Duclous, J. Kirk, K. Bennett, et al., Dense electron-positron plasmas and ultraintense γ-rays from laser-irradiated solids, Phys. Rev. Lett. 108 (2012) 165006.

[40] M. Tamburini, F. Pegoraro, A. Di Piazza, C.H. Keitel, A. Macchi, Radiation reaction effects on radiation pressure acceleration, New J. Phys. 12 (2010) 123005.

[41] Z.-M. Sheng, K. Mima, Y. Sentoku, M.S. Jovanović, T. Taguchi, et al., Stochastic heating and acceleration of electrons in colliding laser fields in plasma, Phys. Rev. Lett. 88 (2002) 055004.

[42] W.P. Leemans, C.G.R. Geddes, J. Faure, C. Tóth, J. van Tilborg, et al., Observation of terahertz emission from a laser-plasma accelerated electron bunch crossing a plasma-vacuum boundary, Phys. Rev. Lett. 91 (2003) 074802.

[43] H.-C. Wu, J. Meyer-ter-Vehn, J. Fernández, B.M. Hegelich, Uniform laser-driven relativistic electron layer for coherent thomson scattering, Phys. Rev. Lett. 104 (2010) 234801.